Research Article

Optics EXPRESS

Laser crystallized low-loss polycrystalline silicon waveguides

YOHANN FRANZ,[1] ANTOINE F. J. RUNGE,[1,2] SWE Z. OO,[1,3] GREGORIO JIMENEZ-MARTINEZ,[1] NOEL HEALY,[4] ALI KHOKHAR,[1] ANTULIO TARAZONA,[1] HAROLD M. H. CHONG,[3] SAKELLARIS MAILIS,[1] AND ANNA C. PEACOCK [1,*]

[1] *Optoelectronics Research Center, University of Southampton, Highfield, Southampton, Hampshire SO17 1BJ,UK*
[2] *Currently with the Institute of Photonics and Optical Science (IPOS), School of Physics, University of Sydney, NSW, Australia*
[3] *School of Electronics and Computer Science, University of Southampton, Highfield, Southampton, Hampshire SO17 1BJ, UK*
[4] *Emerging Technology and Materials Group, Newcastle University, Merz Court, Newcastle, NE1 7RU, UK*
[*] *acp@orc.soton.ac.uk*

Abstract: We report the fabrication of low-loss, low temperature deposited polysilicon waveguides via laser crystallization. The process involves pre-patterning amorphous silicon films to confine the thermal energy during the crystallization phase, which helps to control the grain growth and reduce the heat transfer to the surrounding media, making it compatible with CMOS integration. Micro-Raman spectroscopy, Secco etching and X-ray diffraction measurements reveal the high crystalline quality of the processed waveguides with the formation of millimeter long crystal grains. Optical losses as low as 5.3 dB/cm have been measured, indicating their suitability for the development of high-density integrated circuits.

1. Introduction

Over the past two decades, silicon photonics has emerged as a promising solution for the realization of high performance, high density photonic integrated circuits [1,2]. Using the intrinsic properties of silicon and the mature CMOS technology processes, a wide range of integrated devices with outstanding performances have been demonstrated including modulators [3], lasers [4] and broadband oscillators [5]. Owing to its low optical loss and excellent electronic properties, crystalline silicon (c-Si) remains the most widely used form of this material to date. However, the c-Si platforms present several challenges when considering their integration with electronics, or even for the development of space saving 3D photonic circuits. For example, the fabrication of multi-layer c-Si structures typically requires the use of expensive and technically challenging wafer bonding processes [6].

To overcome these limitations, significant efforts have been devoted to developing alternative, more flexible deposited materials such as hydrogenated amorphous silicon (a-Si:H) [7], silicon nitride (SiN) [8] or polycrystalline silicon (poly-Si) [9]. This work has led to the production of a-Si:H and SiN waveguides exhibiting similar or even lower optical losses than c-Si, which has allowed for the demonstration of several all-optical processing functions in integrated systems [10, 11]. However, a-Si:H and SiN have significantly inferior electronic properties compared to c-Si, which strongly limits their use for the fabrication of integrated devices with electronic capabilities. On the other hand, poly-Si materials have the potential to exhibit both optical and electronic functionalities that are comparable with c-Si, but so far its optical performance has been limited due to fabrication drawbacks. In particular, to obtain good quality

poly-Si directly, the deposition temperature needs to be higher than 900 °C [12–14]. Such high temperatures are incompatible with many CMOS processes and devices that can degrade around 450 °C [15], resulting in a drive to develop lower temperature methods. However, when deposited at low temperatures poly-Si materials typically form small crystals with numerous grain boundaries that act as scattering and absorption points [16]. This results in relatively high optical losses, which have remained a limiting factor for the application of this material in photonic systems [9, 12, 13].

In this paper, we demonstrate the fabrication of low-loss poly-Si waveguides via localized laser crystallization of micron-size stripes of low temperature deposited amorphous silicon (a-Si). We have found that pre-patterning the photonic structures before crystallization helps to confine the thermal energy and results in the formation of long crystal grains, with minimal heat transfer to the surrounding substrate or cladding [17]. Furthermore, it allows for the fabrication of poly-Si devices with a thermal budget < 400 °C, opening a route for their use in multi-layer photonic integration and back-end integration with electronics [9]. The crystal quality of the processed material has been assessed through micro-Raman spectroscopy, Secco etching and X-ray diffraction (XRD) measurements, with the waveguides displaying quasi-single crystal characteristics over millimeter lengths. Finally, optical transmission measurements have revealed a linear loss value as low as 5.3 dB/cm, paving the way for the development of high performance optoelectronic devices.

2. Fabrication

The fabrication process begins with the formation of a thermally grown buried oxide (BOX) layer on top of the c-Si substrate to optically isolate the future waveguides from the silicon base. A thin film of a-Si is then grown using a hot-wire chemical vapor deposition (HWCVD) technique with silane (SiH_4) as the only precursor. HWCVD was preferred over low pressure and plasma-enhanced chemical vapour deposition (LPCVD and PECVD) techniques as it allows for low temperature deposition [15], in this case 320 °C, with low hydrogen concentration. Minimizing the hydrogen content is important to avoid issues associated with violent out-diffusion during laser processing. A schematic of the unprocessed sample is shown in Fig. 1(a), where the a-Si film thickness is ~ 480 nm and the oxide layer is 4.6 µm. Following the deposition, e-beam lithography and plasma etching were used to pattern a series of straight waveguides with widths of 0.5 µm, 1 µm, 1.5 µm and 2 µm in the a-Si film. An example of a typical patterned structure is shown in Fig. 1(b).

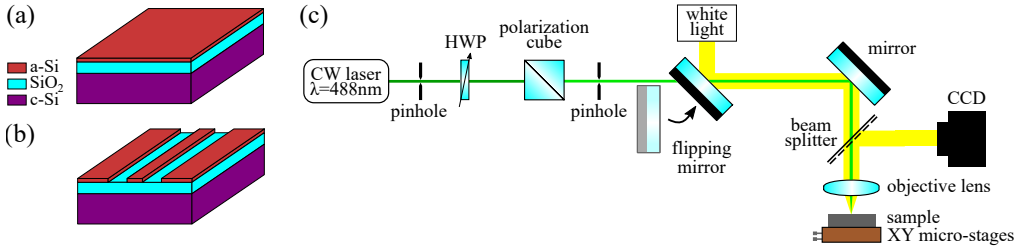

Fig. 1. Schematic of the as-deposited sample before (a) and after (b) patterning of the micron-sized waveguides. The thickness of the a-Si, SiO_2 and c-Si are 480 nm, 4.6 µm and 1 mm, respectively. (c) Schematic of the laser processing setup. HWP, half-wave plate.

The patterned a-Si waveguides were laser processed using the setup schematized in Fig. 1(c). The light source is an argon ion laser emitting continuous wave (CW) radiation at 488 nm with a maximum power of ~ 320 mW, as measured at the sample surface. Although pulsed lasers are more typically used for crystallizing thin film silicon in order to minimize thermal transfer to

the substrate [9], by pre-patterning the samples the volume of a-Si to be processed is reduced thus allowing CW sources to be used without significant substrate heating [17]. Furthermore, the superior power stability of CW sources allows for operation close to the material damage threshold, where grain growth has been shown to be maximal [18]. To avoid distortions of the beam, the power was adjusted using a polarization cube and a half wave plate. The beam was then focused on the top surface of the sample using a 10× objective lens to produce a spot of diameter 4.7 μm. This relatively large spot size was fixed for all experiments as it allows for the optical intensity to be homogeneous across the entire width of the processed waveguides. A pellicle beam splitter, a CCD camera and a white light source were used to image the top of the a-Si waveguides, while a set of two linear micro-precision translation stages allowed for adjustment of the sample position under the laser beam. These stages were used to scan the sample under the laser beam at speeds ranging from 0.01 to 0.1 mm/s while the power was adjusted between 20 mW and 320 mW. As expected, the quality of the laser crystallization strongly depends on the right combination of scanning speed and laser power (generally with higher speeds requiring higher powers) as this controls the melting and cooling rates, both of which are critical for large grain formation [18, 19]. In particular, we observed that for a given scanning speed, the optical power required to melt the material is inversely proportional to the waveguide width. This rather counterintuitive observation can be understood by noting that for narrower waveguides the overlap between the laser beam and the pre-structured silicon material is reduced, thus reducing the overall thermal energy transfer to the waveguides. Moreover, as the width of the waveguide becomes smaller the surface to volume ratio increases, thus accelerating the cooling of the material.

To achieve maximal grain growth it is necessary to completely melt the amorphous material [18, 19]. A direct consequence of this is that surface tension acts to reshape the molten silicon waveguide during the laser processing. This effect is illustrated in Fig. 2, which shows cross-sectional scanning electron microscope (SEM) images of a 2 μm wide waveguide, with Fig. 2(a) before and 2(b) after crystallization, where the processing speed and optical power were 0.1 mm/s and 180 mW, respectively. Before laser crystallization, the a-Si waveguide has a rectangular cross-section, characteristic of the etching process, while the processed waveguide has a semicircular shape. This reshaping induces two key changes to the waveguide. Firstly, the reshaping greatly improves the surface quality, with the 3.58 nm surface roughness of the a-Si waveguides being reduced to 0.52 nm after laser processing, as measured via atomic force microscopy. Secondly, owing to the fact that the poly-Si material has a higher density than a-Si, there is a decrease in the cross-sectional area, with the area before and after processing estimated to be $\sim 0.96\,\mu m^2$ and $\sim 0.83\,\mu m^2$, respectively [17]. We note that the small debris visible in Fig. 2(b) are not due to the laser processing, but arise from multiple polishing of the sample end facets for the optical transmission measurements.

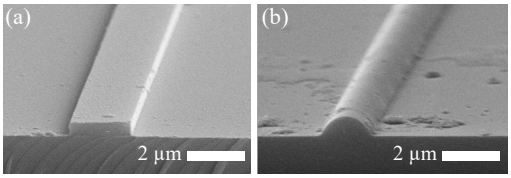

Fig. 2. SEM micrograph cross-section of a 2 μm wide waveguide before (a) and after (b) laser processing. The debris in (b) result from the polishing process.

3. Raman spectroscopy

In order to get an initial assessment of the quality of the laser crystallized silicon waveguides, we performed a set of micro-Raman spectroscopy measurements before and after processing. Examples of Raman measurements obtained with a frequency doubled Nd:YAG laser (532 nm), focused to a spot diameter of 1.2 μm, for different processing conditions are shown in Fig. 3(a). Firstly, the as-deposited material displays a Raman spectrum (yellow line) typical of amorphous silicon, with a broad peak centered at 480 cm^{-1} that consists of several overlapping vibrational modes allowed by the amorphous state. When the laser processing conditions, scanning speed and power combination, are insufficient to completely melt the material, the resulting material consists of small micro and nano-crystalline grains [20]. Compared to single crystal silicon, which has a Raman peak position of 520 cm^{-1} and a width of $\Gamma = 2.7\ cm^{-1}$, the spectra associated with such low quality poly-silicon consists of a broader peak, shifted to shorter wavenumbers, with an asymmetric tail extending over the amorphous vibrational modes. An example of such a material is shown as the orange spectrum in Fig. 3(a), which corresponds to a 2 μm wide waveguide processed with 34 mW of power at a speed of 0.07 mm/s. Finally, when the laser crystallization is optimized, the peak becomes narrower and shifts toward the single crystal reference position. This is illustrated by the blue spectrum of Fig. 3(a), which corresponds to a 1.5 μm wide waveguide processed with 230 mW at 0.1 mm/s. It is important to note that the Raman spectra measured for our samples consist of contributions from both the crystalline substrate and the poly-Si waveguide. Thus, to estimate the linewidth and position of the poly-Si materials accurately, the two peaks first have to be deconvolved and the substrate peak subtracted. The isolated poly-Si peak is then fit using a Voigt function to account for the Gaussian broadening induced by the spectrometer optics and the Lorentzian corresponding to the intrinsic response from the material [21]. The Lorentzian peak width for the low-quality poly-Si peak (orange curve) was measured to be $\Gamma = 3.94 \pm 0.12\ cm^{-1}$, centered at 515 cm^{-1}, whilst the high-quality poly-Si peak (blue curve) was $\Gamma = 2.74 \pm 0.12\ cm^{-1}$, centered at 517 cm^{-1}. For comparison the Raman spectrum for the deconvolved high-quality poly-Si peak is shown together with the c-Si reference in the inset of Fig. 3(a). The fact that the peak widths are so close indicates that this poly-Si waveguide consists of crystals larger than the Raman laser spot resolution. In this instance, the difference in the two peak positions is not related to the grain size, but most likely due to tensile stress in the processed material arising from the volume contraction and geometrical reshaping, as observed in Fig. 2(b) [17].

4. Secco etching

Subsequent to these measurements, Secco etching was undertaken on sacrificial samples to directly reveal the size and quantity of crystals within waveguides processed under these different conditions, as illustrated in Fig. 3(b)-(d). The Secco etch solution consists of an oxidizer, potassium dichromate ($K_2Cr_2O_7$) that converts the weak Si-Si bonds at the grain boundaries into SiO_2, and hydrofluoric acid (HF), which then dissolves the SiO_2, with a 1:2 ratio [22]. The solution was diluted 10 times in water to have a better control of the etching time, which was typically 2 min per waveguide. In Fig. 3(b), the waveguide corresponds to a material quality similar to the orange spectrum in Fig. 3(a), clearly showing a large number of micro/nano-scale grains. By increasing the power to 180 mW, larger (few micron scale) grains can be obtained in the middle of the waveguide, as seen in Fig. 3(c) , but smaller grains still occur at the edges due to the faster cooling rate in these regions. In fact, in this case it is the edges that crystallize first and then these grains act as seeds for the larger grains in the center [23, 24]. Finally, the material in Fig. 3(d) corresponds to the blue spectrum in Fig. 3(a), obtained for the highest processing power. In this particular case it was hard to observe any grain boundaries in the waveguide and, in the section shown here, only two boundaries can be seen separated by ~ 10 μm. Moreover, it

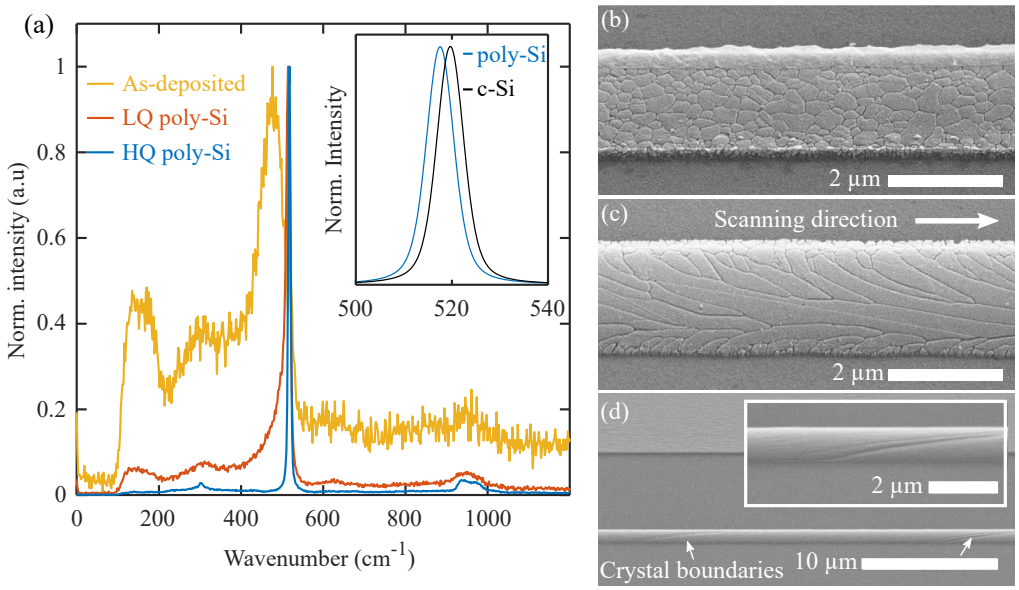

Fig. 3. (a) Raman spectra of the as-deposited a-Si material (yellow), together with a 2 µm wide low-quality poly-Si waveguide (processed at 0.07 mm/s with 34 mW - orange) and a 1.5 µm wide high-quality poly-Si waveguide (processed at 0.1 mm/s with 230 mW - blue). Inset: close up view of the high-quality poly-Si peak together with the c-Si reference. SEM micrographs of waveguides processed to have (b) small (0.07 mm/s and 34 mW), (c) medium (0.1 mm/s and 180 mW) and (d) large polycrystalline grains (0.1 mm/s and 230 mW), as revealed via Secco etching. Inset shows a close up image of the large crystals waveguide.

is clear from the close up image in Fig. 3(d) that the crystal grains that have formed span the entire width of the waveguide (i.e., there are no nano-crystalline regions at the edges), and thus we would expect such a structure to exhibit high quality optical transmission. For the results presented and discussed below we only considered waveguides processed with highest scanning speed (0.1 mm/s) and power combination available to us. Although this speed is lower than desired for large scale processing, previous results obtained for laser processing of thin a-Si films suggest that more practical speeds (tens of mm/s or greater) could be employed with the high stability, high power sources used in manufacturing processes [18].

5. X-ray diffraction

To build up a more complete picture of the crystal quality of the waveguides over long (several millimeter) lengths, we made use of a high-energy micro-focused X-ray beam generated from a synchrotron light source to perform a set of diffraction measurements. The schematic of the X-ray diffraction (XRD) experimental setup is shown in Fig. 4(a). The X-ray beam, at a wavelength of 0.738 Å, was focused on the side of the poly-Si waveguides in a grazing incidence geometry and both the reflected and diffracted beams were recorded on a CMOS detector, as seen in Fig. 4(b). The grazing incident orientation was chosen to minimize the interaction of the X-ray beam with the crystalline substrate, though a large bright spot associated with this can still be seen on the crystalline plane <311>, as shown in Fig. 4(b). As the position of each diffracted spot provides information about the space between atomic layers of the crystal (d-space) and the crystal orientation, we can build up a picture of the number of grains in a given area of our waveguide by the number of spots visible in the pattern. By scanning the probe beam along the waveguide structure, the length of the different crystal grains can be obtained.

XRD measurements were performed using an incident X-ray beam profile of $4 \times 3\,\mu m$, which became $\sim 30 \times 3\,\mu m$ in grazing incidence, with the longest axis aligned along the waveguide length. Thus each diffraction pattern displays crystallographic information for a $30\,\mu m$ long section of the waveguide. Diffraction patterns for the different laser crystallized waveguides were recorded every $200\,\mu m$, over lengths of several millimeters, allowing for the estimation of the average crystals size within the waveguides. Figure 4(b) shows a typical recorded diffraction pattern, where only a single diffraction spot was observed from the poly-Si waveguide, in this case along the <400> crystallographic plane (see circled spot). These results, taken with the Secco measurements in Fig. 3(d), are a strong indication that we have produced crystals that span the entire waveguide width over lengths of at least $30\,\mu m$. A summary of the best crystallization conditions obtained for laser processed waveguides of various widths ($0.5\,\mu m$ through to $2\,\mu m$) is shown in the table of Fig. 4(c). For the 2 and $1.5\,\mu m$ wide waveguides, processed with powers of 180 and 230 mW, respectively, the maximum crystal length are >1 mm, supporting the high crystallization quality suggested by Raman spectroscopy. For the smaller waveguide widths of 1 and $0.5\,\mu m$, processed with 270 and 310 mW, respectively, the crystallization looks promising, but is not quite as good as the larger guides. We attribute this to the fact that the smaller waveguides require higher laser processing powers than what was available to us. Finally, Fig. 4(c) shows that at present no preferential crystalline orientation has been observed in the resulting poly-Si waveguides. However, it is possible that the orientation could be controlled by modifying the growth conditions, for example by adding a silica capping layer or adjusting the cooling rate [25], and this will be investigated in future work.

(a)

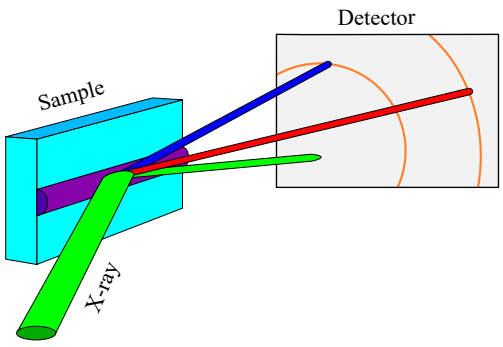

(b)

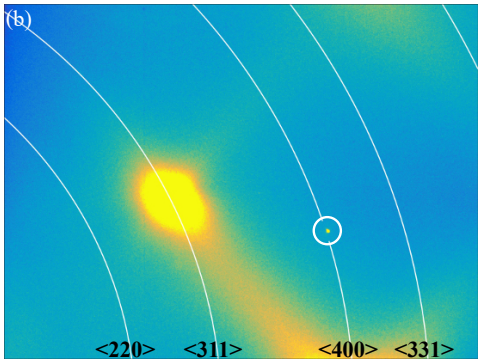

(c)

Waveguide width (μm)	Laser processing		Crystal orientations	Maximum crystal length (mm)
	Power (mW)	Speed (mm/s)		
2	180	0.1	<220>,<331>	1.8
1.5	230	0.1	<220>,<331>,<400>	1.6
1	270	0.1	<311>,<400>,<331>	0.6
0.5	310	0.1	<220>,<331>,<422>	0.8

Fig. 4. (a) Schematic of the XRD experimental setup. (b) Example of the diffraction pattern measured on the CMOS detector for a $1.5\,\mu m$ wide poly-Si waveguide processed at 0.1 mm/s with 230 mW. The large bright spot corresponds to the c-Si substrate and the XRD spot corresponding to the waveguide is circled. (c) List of observed crystal orientations and their crystal grain lengths for different waveguide widths.

6. Transmission losses

Finally, the optical quality of the two larger poly-Si waveguides reported in Fig. 4(c) was assessed by measuring the linear propagation losses using a standard cutback technique. Although these

waveguides support multiple TE modes (~ 5 or more) , these larger dimensions are more suited for characterizing the losses of the processed poly-crystalline material as the light is well confined to the core, reducing contributions from the interface and light guided in the substrate/cladding. To illustrate this, Fig. 5(a) shows the mode profile of the fundamental TE mode in a 2 µm wide waveguide calculated for a wavelength of 1550 nm, as used in the experiments. Light from a TE polarized CW laser diode was coupled into the waveguides using a 60× microscope objective (MO) lens with a numerical aperture (NA) of 0.85, and collimated on a power-meter for collection at the output using a 25× MO lens (NA=0.2). Infrared CCD cameras were used at both the input and output facets to help optimize coupling into the fundamental mode. Figure 5(b) shows the far field output mode for the 2 µm waveguide, confirming that the light is well confined to the core. Cutback measurements were then performed by repeatedly polishing off ~ 1 mm sections of the samples and recording the transmission as a function of length. The results of these measurements are shown in Fig. 5(c), where the loss values for the 1.5 µm (blue) and 2 µm (orange) wide waveguides are 5.31 dB/cm and 6.23 dB/cm, respectively. These transmission losses represent a significant reduction compared to values previously reported for low temperature (< 450 °C) laser processed poly-Si materials, which were estimated to be ~ 20 dB/cm [9]. Indeed, such losses indicate that the formation of millimeter long crystals greatly reduces the absorption and scattering points within the material. We expect that further increases in the grain size will result in even lower losses being achievable. Future work will also focus on optimizing the growth in the waveguides with smaller dimensions, particularly those with the 500 nm widths to access the single mode conditions preferred in integrated circuits.

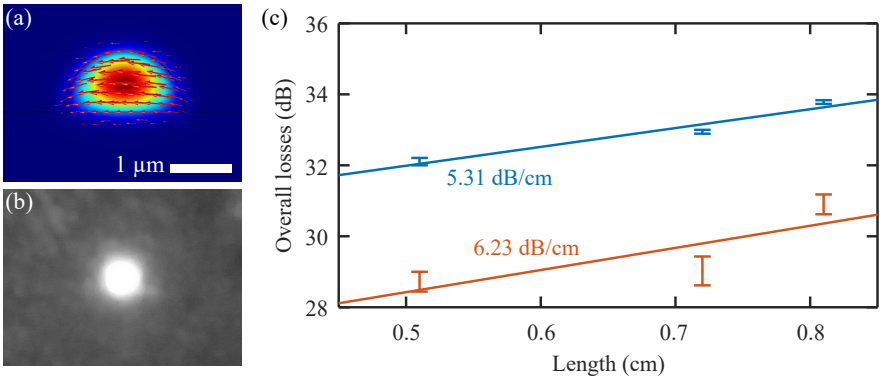

Fig. 5. (a) Fundamental TE mode profile calculated for a 2 µm wide waveguide at a wavelength of 1550 nm (red arrows indicate the electric field). (b) Far field output mode profile measured from a 2 µm wide waveguide using an infrared camera. (c) Cutback loss measurements for i) a 1.5 µm wide waveguide processed with a laser power of 230 mW (blue) and ii) a 2 µm wide waveguide processed with 180 mW (orange). In both cases the scan speed is 0.1 mm/s.

7. Conclusion

In conclusion, we have reported the fabrication of laser crystallized, low-loss and low temperature deposited poly-Si waveguides. A key feature of our technique is the low thermal budget, which makes it compatible with CMOS fabrication processes and multi-layer architectures without the need for wafer bonding. Furthermore, this method is highly flexible in that it could be applied to different amorphous semiconductor materials deposited on a wide range of substrates [26]. The high crystalline quality of the laser processed material has been assessed using micro-Raman spectroscopy, Secco etching and XRD measurements, with the observation of large crystals up to

1.8 mm in length. Finally, the low linear losses of ~ 5 dB/cm of the waveguides obtained with this method indicate that these materials could find numerous applications within high density integrated photonic circuits.

Funding

Engineering and Physical Sciences Research Council (EPSRC) (EP/M022757/1, EP/N013247/1).

Acknowledgments

Portions of this work were presented at the Conference on Lasers and Electro-Optics in 2017, Laser annealing of low temperature deposited silicon waveguides (CLEO_SI.2017.SM3K.4). The authors thank Stuart MacFarquhar for help with the roughness measurements and Dr. K. Ignatyev along with Diamond Light Source staff for their assistance on beamline I18 (SP13025) that contributed to the results presented here. The data for this work is accessible through the University of Southampton Institutional Research Repository (DOI:10.5258/SOTON/D0752).

References

1. G. T. Reed, "Device physics: the optical age of silicon," Nature **427,** 595–596 (2004).
2. B. Jalali, S. Fathpour, "Silicon photonics," J. Lightw. Technol. **24,** 4600–4615 (2006).
3. G. T. Reed, G. Mashanovich, F. Y. Gardes, and D. J. Thomson, "Silicon optical modulators," Nat. Photonics **4,** 518–526 (2010).
4. H. Rong, R. Jones, A. Liu, O. Cohen, D. Hak, A. Fang, and M. Paniccia, "A continuous-wave Raman silicon laser," Nature **433,** 725–728 (2005).
5. B. Kuyken, X. Liu, R. M. Osgood, R. Baets, G. Roelkens, and W. M. Green, "A silicon-based widely tunable short-wave infrared optical parametric oscillator," Opt. Express **21,** 5931–5940 (2013).
6. C. Kopp, S. Bernabe, B. B. Bakir, J. M. Fedeli, R. Orobtchouk, F. Schrank, H. Porte, L. Zimmermann, and T. Tekin, "Silicon photonic circuits: on-CMOS integration, fiber optical coupling, and packaging," IEEE J. Sel. Top. Quantum Electron. **17,** 498–509 (2011).
7. R. Takei, S. Manako, E. Omoda, Y. Sakakibara, M. Mori, and T. Kamei, "Sub-1 dB/cm submicrometer-scale amorphous silicon waveguide for backend on-chip optical interconnect," Opt. Express **22,** 4779–4788 (2014).
8. N. Sherwood-Droz, M. Lipson, "Scalable 3D dense integration of photonics on bulk silicon," Opt. Express **19,** 17758–17765 (2011).
9. Y. H. D. Lee, M. O. Thompson, and M. Lipson, "Deposited low temperature silicon GHz modulator," Opt. Express **21,** 26688–26692 (2013).
10. H. Sun, K. Y. Wang, and A. C. Foster, "Pump-degenerate phase-sensitive amplification in amorphous silicon waveguides," Opt. Lett. **42,** 3590–3593 (2017).
11. Y. Huang, J. Song, X. Luo, T. Y. Liow, and G. Q. Lo, "CMOS compatible monolithic multi-layer Si_3N_4-on-SOI platform for low-loss high performance silicon photonics dense integration," Opt. Express **22,** 21859–21865 (2014).
12. Q. Fang, J. F. Song, S. H. Tao, M. B. Yu, G. Q. Lo, and D. L. Kwong, "Low loss (~6.45 dB/cm) sub-micron polycrystalline silicon waveguide integrated with efficient SiON waveguide coupler," Opt. Express **16,** 6425–6432 (2008).
13. J. S. Orcutt, S. D. Tang, S. Kramer, K. Mehta, H. Li, and V. Stojanović, "Low-loss polysilicon waveguides fabricated in an emulated high-volume electronics process," Opt. Express **20,** 7243–7254 (2012).
14. M. Douix, C. Baudot, D. Marris-Morini, A. Valéry, D. Fowler, P. Acosta-Alba, S. Kerdilès, C. Euvrard, R. Blanc, R. Beneyton, A. Souhaité, S. Crémer, N. Vulliet, L. Vivien, and F. Boeuf, "Low-loss poly-silicon for high performance capacitive silicon modulators," Opt. Express **26,** 5983–5990 (2018).
15. R. E. Schropp, "Present status of micro-and polycrystalline silicon solar cells made by hot-wire chemical vapor deposition," Thin Solid Films **451,** 455–465 (2004).
16. T. M. B. Masaud, A. Tarazona, E. Jaberansary, X. Chen, G. T. Reed, G. Z. Mashanovich, and H. M. Chong, "Hot-wire polysilicon waveguides with low deposition temperature," Opt. Lett. **38,** 4030–4032 (2013).
17. N. Healy, S. Mailis, N. M. Bulgakova, P. J. Sazio, T. D. Day, J. R. Sparks, H. Y. Cheng, J. V. Badding, and A. C. Peacock, "Extreme electronic bandgap modification in laser-crystallized silicon optical fibres," Nat. Mater. **13,** 1122–1127 (2014).
18. J. F. Michaud, R. Rogel, T. Mohammed-Brahim, and M. Sarret, "CW argon laser crystallization of silicon films: structural properties," J. Non-Cryst. Solids **352,** 998–1002 (2006).
19. N. Healy, M. Fokine, Y. Franz, T. Hawkins, M. Jones, J. Ballato, A. C. Peacock, and U. J. Gibson, "CO_2 Laser-induced directional recrystallization to produce single crystal silicon-core optical fibers with low loss," Adv. Opt. Mater. **4,** 1004–1008 (2016).

20. Z. Hu, X. Liao, H. Diao, Y. Cai, S. Zhang, E. Fortunato, and R. Martins, "Hydrogenated p-type nanocrystalline silicon in amorphous silicon solar cells," J. Non-Cryst. Solids **352,** 1900–1903 (2006).
21. L. Lagonigro, N. Healy, J. R. Sparks, N. F. Baril, P. J. Sazio, J. V. Badding, and A. C. Peacock, "Low loss silicon fibers for photonics applications," Appl. Phys. Lett. **96,** 041105 (2010).
22. P. Walker, W. H. Tarn, "Handbook of metal etchants," CRC press (1990).
23. S. J. Park, Y. M. Ku, K. H. Kim, E. H. Kim, B. K. Choo, J. S. Choi, S. H. Kang, Y. J. Lim, and J. Jang, "CW laser crystallization of amorphous silicon; dependence of amorphous silicon thickness and pattern width on the grain size," Thin Solid Films **511,** 243–247 (2006).
24. M. Lee, S. Moon, M. Hatano, K. Suzuki, and C. P. Grigoropoulos, "Relationship between fluence gradient and lateral grain growth in spatially controlled excimer laser crystallization of amorphous silicon films," J. Appl. Phys. **88,** 4994–4999 (2000).
25. J. S. Yun, C. H. Ahn, M. Jung, J. Huang, K. H. Kim, S. Varlamov, and M. A. Green, "Diode laser crystallization processes of Si thin-film solar cells on glass," Eur. Phys. J. PV **5,** 55204 (2014).
26. J. Hu, L. Li, H. Lin, P. Zhang, W. Zhou, and Z. Ma, "Flexible integrated photonics: where materials, mechanics and optics meet," Opt. Mater. Express **3,** 1313–1331 (2013).